frontiers in Chemical Engineering

ORIGINAL RESEARCH
published: 28 May 2021
doi: 10.3389/fceng.2021.683379

Clinical Autopsy of a Reverse Osmosis Membrane Module

Graciela Gonzalez-Gil[1], Ali Reza Behzad[2], Andreia S. F. Farinha[1], Chengyan Zhao[1], Szilard S. Bucs[1], Tariq Nada[3], Ratul Das[4], Thomas Altmann[5], Paulus J. Buijs[1] and Johannes S. Vrouwenvelder[1,6]**

[1]Biological and Environmental Science and Engineering Division (BESE), Water Desalination and Reuse Center (WDRC), King Abdullah University of Science and Technology (KAUST), Thuwal, Saudi Arabia, [2]Advanced Nanofabrication Imaging and Characterization, King Abdullah University of Science and Technology (KAUST), Thuwal, Saudi Arabia, [3]CTO Representative KSA, ACWA Power, Jeddah, Saudi Arabia, [4]ACWA Power Innovation Department, Thuwal, Saudi Arabia, [5]ACWA Power Innovation Department, Dubai, United Arab Emirates, [6]Faculty of Applied Sciences, Department for Biotechnology, Environmental Biotechnology, Delft University of Technology, Netherlands

OPEN ACCESS

Edited by:
Ludovic F Dumée,
Khalifa University, United Arab Emirates

Reviewed by:
Gayathri Naidu,
University of Technology Sydney, Australia
Amani Al-Othman,
American University of Sharjah, United Arab Emirates

***Correspondence:**
Graciela Gonzalez-Gil
graciela.gonzalezgil@kaust.edu.sa
graciella.gil@gmail.com
Johannes S. Vrouwenvelder
johannes.vrouwenvelder@kaust.edu.sa
J.S.Vrouwenvelder@tudelft.nl

Specialty section:
This article was submitted to Separation Processes, a section of the journal Frontiers in Chemical Engineering

Received: 20 March 2021
Accepted: 17 May 2021
Published: 28 May 2021

Citation:
Gonzalez-Gil G, Behzad AR, Farinha ASF, Zhao C, Bucs SS, Nada T, Das R, Altmann T, Buijs PJ and Vrouwenvelder JS (2021) Clinical Autopsy of a Reverse Osmosis Membrane Module. Front. Chem. Eng. 3:683379. doi: 10.3389/fceng.2021.683379

The desalination of seawater using reverse osmosis membranes is an attractive solution to global freshwater scarcity. However, membrane performance is reduced by (bio)fouling. Membrane autopsies are essential for identifying the type of fouling material, and applying corrective measures to minimize membrane fouling. Information from full-scale membrane autopsies guiding improved plant operations is scant in the formal literature. In this case-study, a reverse osmosis membrane from a full-scale seawater desalination plant with a feed channel pressure drop increase of about 218% over the pressure vessel was autopsied. The simultaneous determination of microbial cells, ATP, and total organic carbon (TOC) abundances per membrane area allowed estimating the contributions of biofouling and organic fouling. The abundance of microbial cells determined by flow cytometry (up to 7×10^8 cells/cm^2), and ATP (up to 21,000 pg/cm^2) as well as TOC (up to 98 µg/cm^2) were homogeneously distributed on the membrane. Inorganic fouling was also measured, and followed a similar coverage distribution to that of biofouling. Iron (~150 µg/cm^2, estimated by ICP-MS) was the main inorganic foulant. ATR-FTIR spectra supported that membrane fouling was both organic/biological and inorganic. High-resolution SEM-EDS imaging of cross-sectioned membranes allowed assessing the thickness of the fouling layer (up to 20 µm) and its elemental composition. Imaging results further supported the results of homogeneous fouling coverage. Moreover, imaging revealed both zones with and without compression of the polysulfone membrane layer, suggesting that the stress due to operating pressure was heterogeneous. The procedure for this membrane autopsy provided a reasonable overview of the diverse contributors of fouling and might be a starting point to building a consensus autopsy protocol. Next, it would be valuable to build a RO membrane autopsy database, which can be used as a guidance and diagnostic tool to improve the management and operation of RO desalination plants.

Keywords: reverse osmosis, full scale desalination plant, membrane module autopsy, fouling, biofouling, drinking water, membrane compression

INTRODUCTION

The global demand for freshwater increases constantly (UNESCO UN-Water, 2020). However, the natural replenishment of freshwater, in most regions, is not sufficient to meet current human demands. To address this issue, the production of freshwater through desalination can alleviate water scarcity, but the process is energy-intensive (Mazlan et al., 2016). Nonetheless, decreased costs of materials make desalination an attractive alternative for the production of freshwater in arid regions, as well as in regions with a stressed hydrologic cycle due to climate change.

The preferred method for desalination is via water filtration through reverse osmosis (RO) membranes. Among the available desalination methods, RO is the most effective in terms of energy requirements and unit water cost (Qasim et al., 2019). Current RO desalination plants produce 65.5 million m^3/day, which accounts for 69% of the volume of desalinated water produced worldwide (Jones et al., 2019).

Thin-film composite membranes arranged in spiral-wound modules are the most common units used in RO (Qasim et al., 2019). This membrane consists of a polyamide active layer (0.2 μm thick) supported by polysulfone (40 μm) and polyester fabric layers (120 μm) (Petersen, 1993; Rodríguez-Calvo et al., 2015). The polyamide layer is responsible for the selectivity of the membrane, while the polysulfone interlayer makes it possible that the polyamide withstands high pressures. The polyester layer cannot function as direct support for the polyamide because it is too irregular and porous (Rodríguez-Calvo et al., 2015). Despite improvements in the RO process and membrane technology (Tawalbeh et al., 2018), unwanted deposition of materials on the membrane surface during operation reduces membrane performance. This phenomenon is known as fouling and is currently the weakest link of RO technology.

Based on the nature of the material that deposits on the surface of the membranes, fouling is referred to as particulate fouling, organic fouling, inorganic fouling, and biofouling (Jiang et al., 2017; Flemming, 2020). Fouling reduces the active membrane area and increases membrane resistance. The result is a decline in permeation rate, thus a decline in production. To maintain the production capacity, the feed operating pressure is increased. The operation at increased pressures of fouled RO membranes increases energy demands and costs (Hoek et al., 2008; Ruiz-García and Ruiz-Saavedra, 2015). For example, fouled membranes need frequent chemical cleaning, which reduces the lifespan of the membranes. Ultimately, extreme fouling can influence the quantity and quality of the produced water.

The fouling development and fouling impact on performance is influenced by several aspects, namely: 1) feed water quality such as biodegradable nutrient concentration (Griebe and Flemming, 1998; Vrouwenvelder et al., 2009), chemical dosages (Vrouwenvelder et al., 2000) and water temperature, 2) design of spacer (Siddiqui et al., 2017) and membranes, and 3) RO plant design and operational conditions (cross flow velocity, flux and concentration polarization). Concentration polarization of salts and organics along with biofilm enhanced osmotic pressure phenomena affect membrane performance negatively (Herzberg and Elimelech, 2007; Chong et al., 2008; Radu et al., 2010; Voutchkov, 2010; Zargar et al., 2020). Recently, rapid progress has been made on insights on biofouling development in modules (Creber et al., 2010a; Bristow et al., 2021) and the development of novel feed spacers (Kerdi et al., 2020; Qamar et al., 2021).

Biofouling is predominately localized in the lead elements of the first stage of spiral wound membrane installations (Carnahan et al., 1995; Vrouwenvelder et al., 2011). At the inlet side of the RO membrane installations, biofilm bacteria utilize the biodegradable nutrients. Thus, the amount of biofilm at the concentrate side of the RO plant is typically lower.

The linear velocity of the water in the lead module is highest among the membrane modules located in series in the pressure vessel, indicating that biofilm formation in the lead module has the most impact on membrane performance decline (Vrouwenvelder et al., 2008). The biofilm formation impact on membrane performance indicators is typically sequentially: The feed channel pressure drop increase (DP) is impacted earliest and strongest followed by permeability and salt rejection decline, underlining that feed channel pressure drop is a sensitive and early biofouling monitoring indicator (Siebdrath et al., 2019). Therefore, membrane autopsies should include the lead membrane module. A pressure drop reduction by biofilms in the (lead) membrane element reduces the downstream driving force for water production and possible localized dead zones with increased concentration polarization (Vrouwenvelder et al., 2008; Creber et al., 2010b).

Identifying the causes of fouling is paramount to apply corrective measures. Although fouling is virtually unavoidable, understanding the causes and mechanisms of its development can lead to improved operational and managing strategies aiming at minimizing fouling. Therefore, when fouling occurs, membrane modules are retrieved and examined to determine the cause of fouling—a procedure called membrane autopsy. An autopsy can comprise a diverse set of analyses of the membrane. Each analysis provides distinct information that assists in identifying the cause of membrane failure. Although membrane autopsies are destructive investigations, it is recognized that they result in significant savings in operational costs (Liu et al., 2018). Hence, they are also conducted as a periodical maintenance practice in some installations.

Despite the importance of membrane autopsies (Vrouwenvelder et al., 2003), sparse autopsy studies are available in the literature (Fortunato et al., 2020; Rho et al., 2019; Zheng et al., 2018). The majority of information regarding membrane autopsies refers to laboratory-scale studies, while full-scale studies are scant. For example, in the last 26 years, the total number of records in the Web of Science database for the search Membrane + Autopsy + Reverse Osmosis is 200. However the number of publications, which are relevant for desalination full-scale applications, drops to 20 when the search is done with the terms Membrane + Autopsy + Reverse Osmosis + Full-Scale + Desalination (**Figure 1**). From these, only a few provide information about the layout of the plant and physical and chemical characteristics of the feed water and plant performance (Ruiz-García et al., 2018; Nejati et al., 2019).

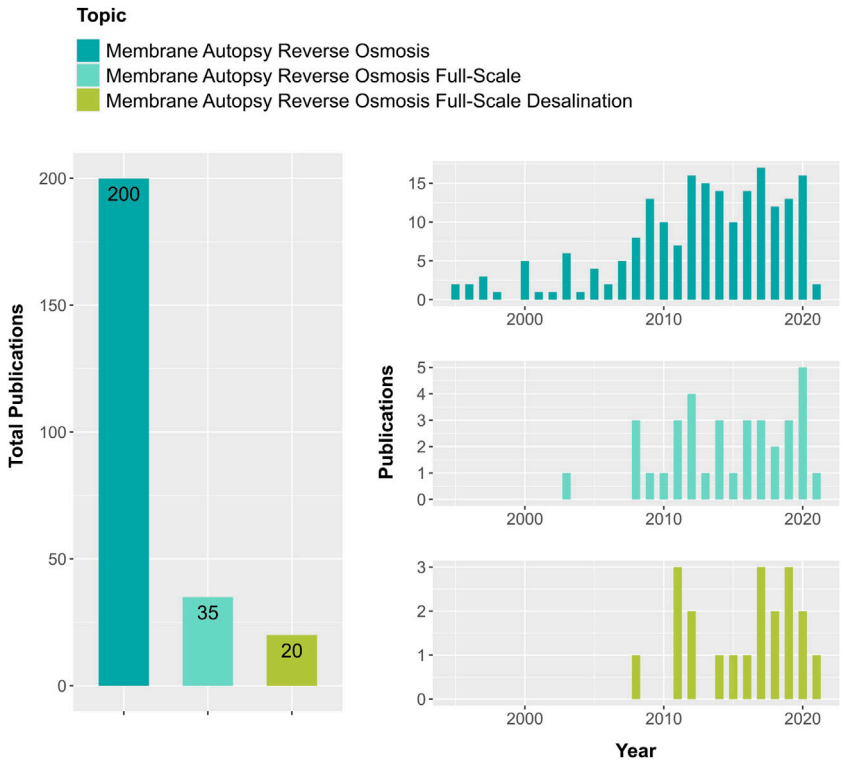

FIGURE 1 | Number of publication records retrieved for different combined topic keywords from the Web of Science database when searched for the year 1995 to February 2021. By including the words full-scale and desalination in the topic of membrane autopsy in reverse osmosis, the number of publications decreased ten times.

Most autopsy studies are conducted by companies and reports are not available.

In most autopsy efforts, conventional approaches are used (Darton et al., 2004; Chesters et al., 2013; Peña et al., 2013), and limited studies determine the different types of fouling simultaneously. Conventional methods include loss-on ignition to discriminate inorganic and organic fouling, and conventional surface analysis using scanning electron microscopy (SEM). When the coverage and type of fouling are spatially heterogeneous, a large number of SEM observations would be required to have a representative picture because conventional SEM probes small areas. In addition, conventional heterotrophic plate counts are used to assess biofouling (Dudley and Darton, 1996; Nejati et al., 2019). This method targets only a minute fraction of cultivable bacteria (Hugenholtz, 2002), hence biofouling would be highly underestimated when this method is used. Current advancements in analytical instruments may allow extracting further information from autopsies. For example, novel multi-beam SEM will allow probing large sample areas (Eberle and Zeidler, 2018). Furthermore, SEM 3D imaging approaches combined with available image analysis algorithms (Sundaramoorthi et al., 2016; Alvarez et al., 2019) can help better understand the ultrastructure properties of the fouling material and the impacted membrane. The quantification of microbial cells contributing to biofouling can be determined by flow cytometry, which is a high throughput method that does not depend on microbial cultivation (Prest et al., 2013; Nescerecka et al., 2016; Van Nevel et al., 2017).

In the present study, the aim was twofold. First, we simultaneously determined the extent of organic fouling, inorganic fouling, and biofouling of a RO membrane from the lead module of a full-scale desalination plant. The extent of biofouling was assessed by quantifying microbial cells using flow cytometry, ATP and TOC. Secondly, and in contrast to the conventional surface examination of fouled membranes by electron microscopy, we explored the information gained when cross-sectioned fouled membranes are examined.

MATERIALS AND METHODS

The layout of the full-scale desalination plant is depicted in **Figure 2**, and feed water parameters are provided in **Supplementary Table S1**.

Following the intake of seawater, sodium hypochlorite (NaOCl) is dosed continuously to maintain chlorine at 1 mg/L. Next, iron chloride ($FeCl_3$, dosed continuously to keep at 6.0 mg/L) and a cationic polyelectrolyte are added to remove suspended solids and colloids. The flocculated material is then removed from the intake water using a multi-media filter (MMF). After the MMF, sodium metabisulfite (SMBS) is dosed to remove chlorine which otherwise would damage the RO membrane. The continuous dose of SMBS is maintained at 0.5 mg/L. After the

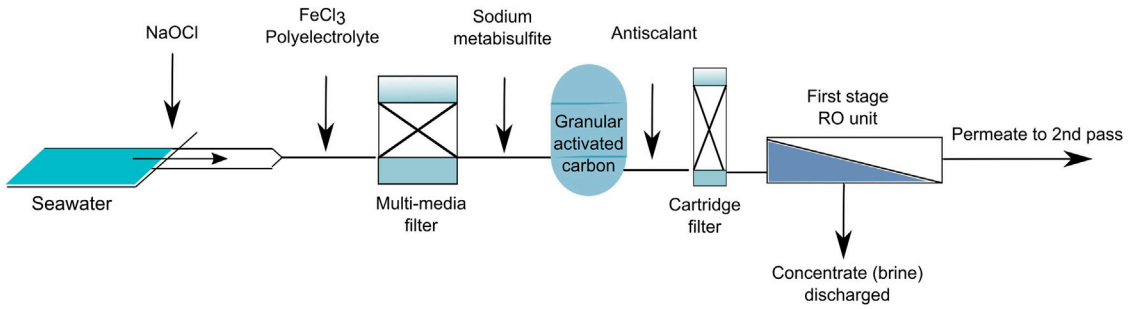

FIGURE 2 | The layout of the full-scale desalination plant showing the location of dosage for different chemicals.

MMF the water passes through a granular activated carbon filter (GAC). After the GAC, a phosphonate-based antiscalant (Berkosafe, Wetiko) is added continuously to maintain its concentration at 3–4 mg/L. Finally, the water passes through a cartridge filter before entering the RO unit.

The cartridge filters are replaced, on average, every 45 days when the differential pressure (DP) reaches 600 kPa. The average cleaning in place (CIP) is conducted every 12 weeks when the DP is about 250 kPa and consists of two phases. Phase 1 comprised: 0.03% sodium lauryl sulfate and 1% Kleen MCT 411 adjusted to pH11 with NaOH, recirculation (1 h), soaking (2 h), and flushing with RO permeate. The Kleen MCT 411 (Suez) used in phase 1 is a mixture of sodium perborate monohydrate (40–60%), sodium tripolyphosphate (20–40%), ethylenediaminetetraacetic acid tetrasodium salt (10–20%), NaOH (2.5–10%), and tetrasodium pyrophosphate (1–2.5%). Phase 2 comprised: 2% citric acid adjusted to pH 2 with HCl, recirculation (1 h), soaking (2 h), followed by flushing with RO permeate.

We retrieved a reverse osmosis membrane module from the lead position of the first stage of this full-scale desalination plant. The membrane was a LG SW 440 High Rejection unit manufactured by LG Chem (serial number AG9A28F1499). On this plant, each train has 20 pressure vessels, seven elements long. The plant operated prior to the cleaning at a feed pressure of 6,197 kPa, and a brine pressure of 5,974 kPa. The differential pressure over the feed channel has increased with time from about 70 to 223 kPa, an increase of about 218%. The permeate and brine flows are 74.4 and 105 m^3/h, respectively. The conductivity of the permeate is 280.4 µS/cm. The RO unit runs at a water recovery of 41.5%. When we retrieved the lead membrane module from a pressure vessel, it was in operation for one year.

Dissection of the Membrane

We processed the membrane module on the same day of retrieval. The case of the membrane module was opened using an electric saw. We inspected and photographed the macroscopic status of all membrane components to assess the extent and distribution of fouling. Then, membrane coupons of defined dimensions were dissected at about 10 cm from the inlet and 10 cm from the outlet side of the membrane. These sections did not contain glue lines. The surface area of coupons (stacked membrane and feed spacer) ranged from 3 to 7 cm^2.

Assessment of the Organic Fouling

To estimate the extent of organic fouling, the total organic carbon (TOC) of membrane coupons was measured. A membrane coupon was placed into a sterile tube containing 40 ml of filtered-sterilized (0.2 µm) milli-Q water. To detach the foulant from the membrane, the sample was sonicated at 4°C for 1 min at 50-amplitude using a sonicator probe (Q700 Qsonica sonicator, United States). The resulting extract was filtered (0.45 µm), and TOC was measured using a total organic carbon analyzer (TOC-VCPH, Shimadzu, Kyoto, Japan).

We used attenuated total reflection Fourier transformed infrared (ATR-FTIR) analysis to identify the functional groups of the organic matter deposited on the membrane surfaces. Membrane coupons were placed in Petri dishes and dried at 40°C for 24 h. Infrared spectra of virgin and fouled coupons were obtained with a Spectrum 100 Optica FT-IR spectrometer (PerkinElmer Inc., Waltham, Massachusetts, United States). Per measurement, 32 scans were recorded over a wavenumber range of 4,000–458 cm^{-1} with a resolution of 4 cm^{-1}.

Assessment of Biofouling

We measured the contents of adenosine triphosphate (ATP) as an indicator of the presence of active microbial cells on the membrane. The fouling material was extracted from the membrane by sonication as specified above. The ATP was analyzed by luminescence resulting from the enzymatic oxidation of D-luciferin by luciferase. Luciferase activity strictly depends on the presence of ATP. The ATP-driven luminescence of the extracted fouling samples was measured using a Celsis Advance II luminometer. The recorded relative light units (RLU) were converted to ATP concentrations using a calibration curve as described previously (Hammes et al., 2010).

The number of microbial cells was determined by flow cytometry from suspensions of detached fouling material from the coupons. Microbial cells in a 700 µl suspension were stained with 7 µl SYBR Green I (Invitrogen, 100 × diluted in 10 mM Tris buffer pH = 8.1), as recommended in (Nescerecka et al., 2016), and incubated 10 min in the dark at 35°C. Then, stained cells were measured by flow cytometry (FCM) using a BD Accuri C6 instrument as described by (Prest et al., 2013). Briefly, the blue 488 nm laser (50 mW) was used to collect the green fluorescence at Fl1 = 533 30 nm, the red fluorescence Fl3 > 670 nm, as well as intrinsic cell parameters given by the side scattered and forward

scattered light signals. The counting hardware of the instrument is calibrated to measure the number of particles in a 50 µl sample volume. Electronic gating was used to separate positive microbial stained signals from instrument, and water background noise. Sterilized filtered (0.2 µm) ultrapure water, as well as unstained samples were used as controls in all runs.

Assessment of Inorganic Fouling

To identify, and estimate the contents of inorganic components in the fouling material, we used inductively coupled plasma mass spectroscopy (ICP-MS). The membrane coupons were immersed in 50 ml of 6% v/v HNO_3, and incubated 24 h at 40°C in a shaker. The samples were then filtered (0.45 µm) and diluted ten times. Elements were analyzed using an ICP-MS (Agilent 7500cx, Agilent Technologies, United States), and quantification was based upon calibration by a series of external standards. All elements were acquired in helium collision mode.

Scanning Electron Microscopy and Energy-Dispersive X-Ray Spectroscopy Analyses

We conducted SEM to examine the ultrastructure of fouling formed on the membrane surface. SEM-EDS analyses were used to determine and map the elemental composition of the fouling materials. To preserve the fouling materials for SEM imaging and EDS analyses, small pieces of the fouled membrane were freeze dried (K775X Turbo Freeze Drier, Quorum Technologies, United Kingdom). To prepare cross-sections of freeze dried samples, small pieces of the membrane were immersed in liquid nitrogen and then were fractured. Fractured membranes were mounted on a 45° pre-tilted aluminum stub. To dissipate charging during SEM imaging and EDS analysis, samples were coated with 5 nm iridium using Q150T S Sputter coater (Quorum Technologies, United Kingdom). A Teneo VS SEM (Thermo Fisher Scientific, Netherlands) equipped with a secondary and backscattered detectors (ETD and T1 detectors), and an energy dispersive spectroscopy (EDS) detector was used for imaging and EDS analysis of inorganic elements. SEM images were acquired at an accelerating voltage of 1 kV and 9–10 mm working distance in optiplan mode. EDS analysis and mapping were done at an accelerating voltage of 14 kV and 10 mm working distance in analytical mode.

RESULTS

Macroscopic Inspection of the Membrane

An inspection of the spiral wound RO membrane module revealed no macroscopic damage to the outer module components, and there was no telescoping of the membrane. After the destructive opening of the membrane module, the unwound membrane sheets were visually inspected: Visible membrane defects or glue-line damage were absent. An orange-colored fouling material 1) was homogeneously distributed over the membrane sheets, and 2) covered all individual membrane sheets of the membrane module (**Figure 3**).

Organic Material and Biofouling Indicators

Results of TOC, ATP, and cell counts accumulated on the feed spacer and membrane evidenced the presence of organic and biological fouling (**Figure 3**). The TOC contents on the inlet and outlet samples differed significantly ($p = 0.032$), with the inlet samples containing higher amounts of organic material. However, as a whole, the TOC ranged from 75 to 98 µg/cm^2, and inlet and outlet TOC values were in the same order of magnitude (**Figure 4A**).

The ATP contents, and the number of microbial cells in the inlet and outlet random samples did not differ significantly ($p > 0.05$). The ATP values varied between 6,500 and 21,000 pg/cm^2 (**Figure 4B**). The number of microbial cells varied between 2.0 and 3.5 × 10^8 cells/cm, with the highest value of 7 × 10^8 cells/cm detected in the inlet zone (**Figure 4C**).

Compared to the infrared spectra of a virgin membrane, the fouled membrane module showed distinct differences (**Figure 5**), indicating that organic fouling occurred. Infrared spectra of the fouled membrane showed the presence of characteristic carbohydrates peaks (1,000–1,100 cm^{-1}). Furthermore, amide I and amide II peaks attributed to proteins were also detected (1,600–1700 cm^{-1}). The higher absorption peak at 3,300 cm^{-1} in the fouled membrane confirms the presence of carbohydrates as this band is due to the OH stretch. Moreover, a peak in the inorganic region at 458 cm^{-1} was likely from the presence of iron (**Figure 5**).

Inspection of the Membrane and the Fouling Cake Layer at High Magnification

The general structure of the membrane and the fouling cake layer was inspected using SEM. We examined coupon samples and diverse fields of view, and consistently, the fouling cake layer covered the membrane homogeneously (**Figure 6**). The thickness of the fouling cake layer ranged from about 3 to 20 µm. Apparently compression of the polysulfone layer occurred during operation. The polysulfone was barely visible at some points along the membrane (**Figure 6A**, arrows, see also **Supplementary Figure S1**). In contrast, an inspection of a virgin membrane showed a well-defined polysulfone layer (**Figure 7A**), and a pristine polyamide (**Figure 7B**). The polyamide was completely covered by the cake layer in the fouled membrane (**Figure 6B**).

Moreover, we noticed two polysulfone structures on the polysulfone layer of the fouled membrane (**Supplementary Figure S2**). One was laminar-like (**Figure 6C**) while the other was spongy-like (**Figure 6D**). Analysis of the virgin membrane showed that these two distinct polysulfone structures were arranged one on top of the other along the membrane (**Figures 7C,D**). However, in the fouled membrane, we observed zones with either laminar-like (**Figure 6C**) or the spongy-like (**Figure 6D**) polysulfone structures. This indicates that the compression of the polysulfone layer in the fouled membrane was not homogeneous. The points of compression seemed to correspond to undulations observed on the membrane (arrows in **Figure 6A**), and these undulations may correspond to the geometry of the 28 mil (~710 µm thick) spacer.

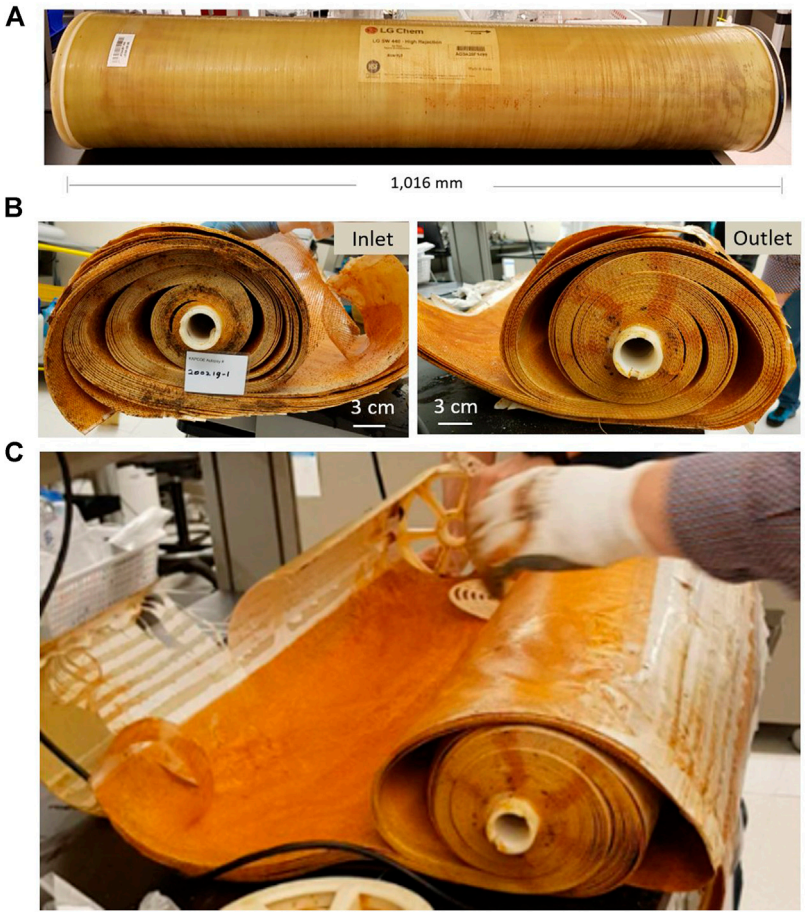

FIGURE 3 | Macroscopic status of the membrane module. **(A)** Intact membrane case. **(B)** Frontal view of the inlet and outlet after opening the module and removing the end-caps. **(C)** Unwound membrane sheet illustrating homogeneous coverage of the membrane sheet by orange-colored fouling material.

Elemental Composition of the Fouling Material

To understand better the fouling of the membrane, we first examined the elemental composition of a virgin membrane using energy-dispersive X-ray spectroscopy analysis (EDS). The surface, made of polyamide, distinctively contained about 3–4% of nitrogen (**Table 1**). An estimate of the nitrogen in the virgin membrane is important since this element can be an indicator of organic (bio) fouling when examining a fouled membrane. Moreover, results of the elemental map suggest the presence of two distinct polysulfone layers. One with a sulfur content of about 2–3% (low sulfur layer), and one with a sulfur content of about 10–16% (high sulfur layer). The physical appearance of these polysulfphone layers was also distinct (**Figure 7D**). The high sulfur layer had a laminar-like appearance, while the low sulfur layer was spongy-like (see *Inspection of the Membrane and the Fouling Cake Layer at High Magnification*).

On the other hand, the cake layer from the inlet and outlet contained nitrogen contents at about 11–15% (**Table 1**, **Supplementary Tables S3–S4**), which contrast with the nitrogen content of about 4% of the virgin membrane surface (**Table 1**), and supports that organic (bio) fouling was present on the fouled membrane.

In addition, the EDS results showed that Fe was an important fouling component (about 6–7%, **Table 1**). A quantitative assessment of the inorganic contents of the fouling material by ICP-MS showed that the Fe content on the membrane and spacer was about 150 $\mu g/cm^2$ (**Supplementary Table S5**).

When conducting an autopsy of a desalination RO membrane, we need to assess whether the presence of sodium in the fouling material originates from remnants of seawater as heavy scaling by Na minerals would be rare. The assessed Na contents found in this membrane may originate from remnants of seawater since its ratio with respect to the presence of other elements closely resemble those found in seawater (**Table 2**).

DISCUSSION

Membrane autopsies are often conducted when the performance of a membrane installation decrease. The feed channel pressure

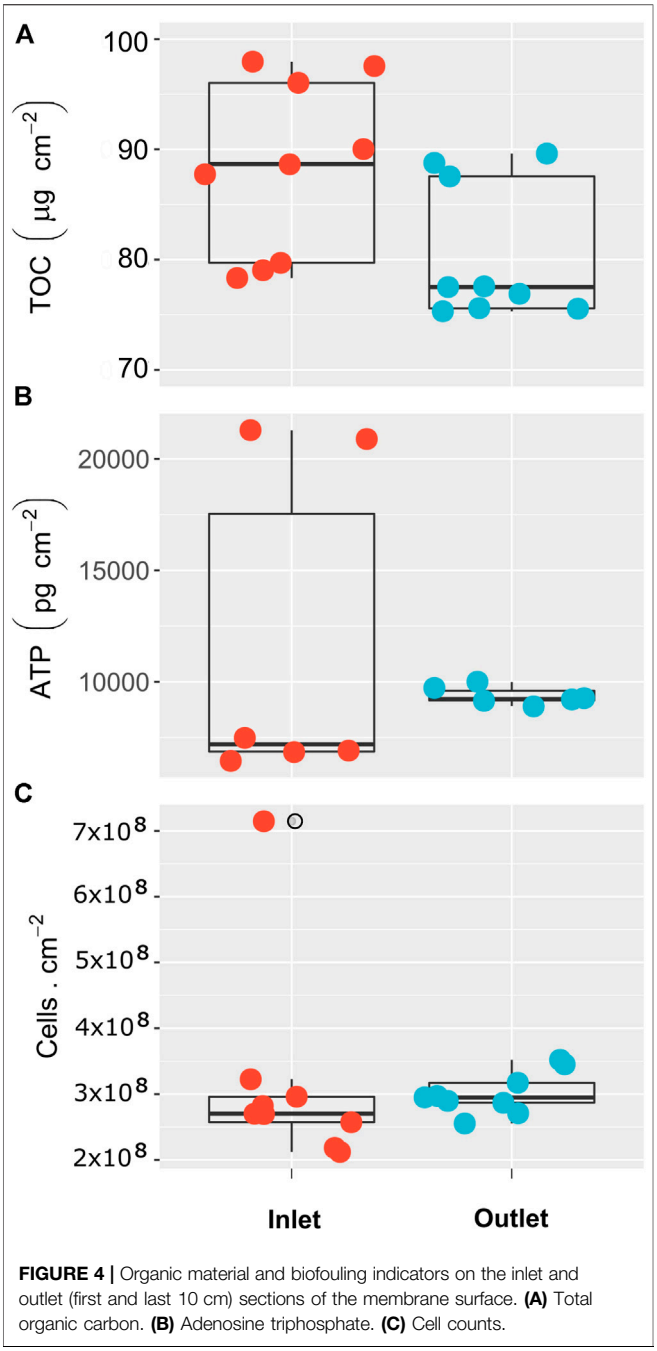

FIGURE 4 | Organic material and biofouling indicators on the inlet and outlet (first and last 10 cm) sections of the membrane surface. **(A)** Total organic carbon. **(B)** Adenosine triphosphate. **(C)** Cell counts.

drop over the pressure vessel containing the studied membrane had increased about 218%, suggesting important flow channeling or blockage of the spacer channel (dead zones). This could result in decreased permeate production and quality (Hijnen et al., 2009; Vrouwenvelder et al., 2009; Kucera, 2019). The decline in pressure means that the driving force to produce water has been reduced.

Since practitioners now realize that the information gained through autopsies translates into considerable operational cost savings, membrane autopsies are increasingly conducted for operation optimization and routine monitoring.

There is no standard procedure or set of analytical methods to conduct membrane autopsies. This limits the comparisons and translation of results to different membrane fouling cases. Here, we explored using some advanced methods to assess the physical status of the membrane and to determine the extent of the different fouling types.

Organic Fouling and Biofouling Are Moderate to Severe

Although comparisons are not straight forward, if one considers the reported TOC and ATP values—which are in all cases measured by the same approaches, combustion catalytic oxidation and luminescence, respectively—the extent of organic fouling and biofouling in this membrane was important when compared to previous autopsies data (**Table 3**).

Considering a value of 8.9×10^{-17} g ATP/cell (Hammes et al., 2010), we can calculate the number of active cells based on the measured maximum ATP value of 21,000 pg/cm^2 for the studied membrane. The number of active cells would be about 2.4×10^8/cm^2, which three times lower than the measured maximum total cell counts of 7×10^8/cm^2. This suggests that about most of the cells on the membrane were probably not active. Although the use of propidium iodide as a stain in combination with SYBR Green to determine the number of active cells has limitations, we propose using it in future autopsies to gain rough estimates on the proportion of total and intact microbial cell numbers. This information is relevant in cases where the effectiveness of specific pretreatments or membrane cleaning procedures need investigation.

Assuming that all TOC would be due to microbial cells, we can estimate the number of microbial cells based on the measured average TOC content of 80 µg/cm^2, and considering a carbon content of 39 fg C/cells (Vrede et al., 2002). The estimated cell number would be about 2×10^9/cm^2, which would be about six to ten times higher than the cell counts we measured by flow cytometry. This suggests an important contribution of organic fouling.

Since the membrane itself has organic components, ATR-FTIR analysis of fouled membranes can be challenging, particularly when the fouling is mild. Here, fouling was important as reflected by the performance declined and the ATR-FTIR spectra of fouled and virgin membranes contrasted (**Figure 5**). The ATR-FTIR spectra support that the fouling of the membrane was both organic/biological and inorganic. In the case of mild fouling, an option for the analysis of the fouling material would be to dry the membrane sample, scrap the fouling material, and then analyze it. This would eliminate the interference of the membrane signals.

Taken together, our results and two previous studies (Rehman et al., 2019; Fortunato et al., 2020) indicate that biofouling can occur on RO membranes desalinating Red Sea water.

Iron Deposits Caused Severe Fouling

Another important contributor to the fouling of this membrane was Fe. The EDS analysis over various areas of the inlet and outlet sections of the membrane showed that the distribution of Fe was

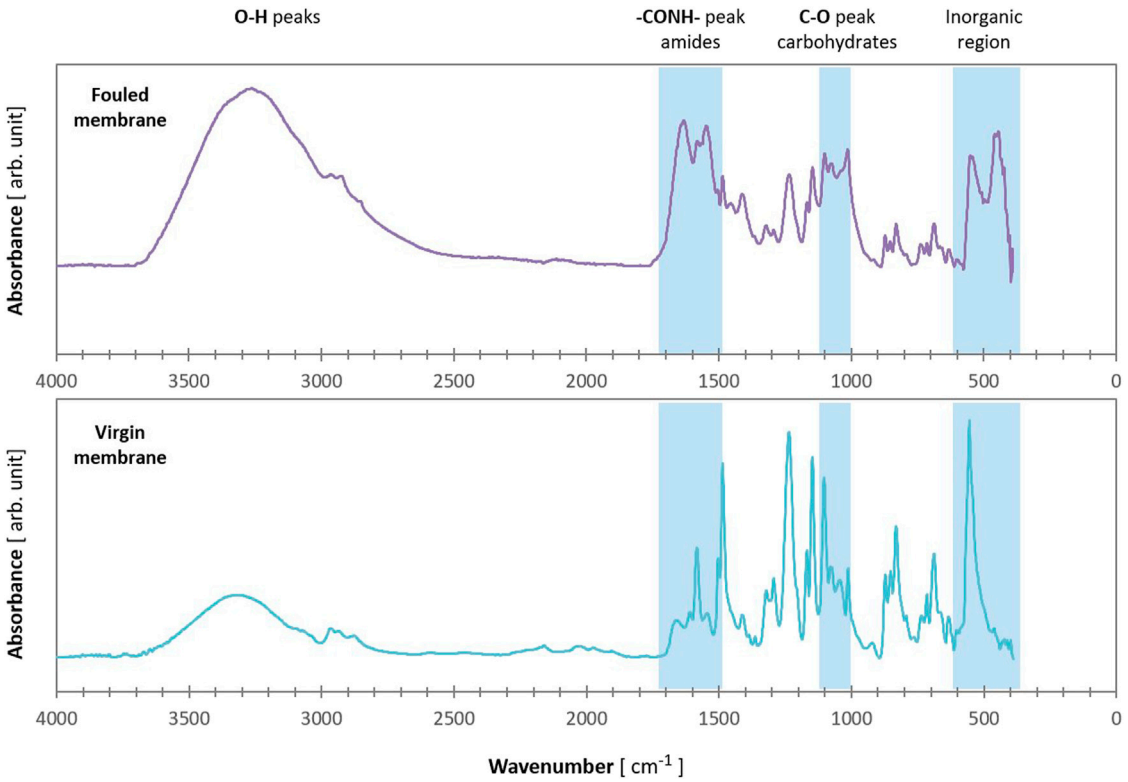

FIGURE 5 | Infrared spectra of fouled and virgin reverse osmosis membrane.

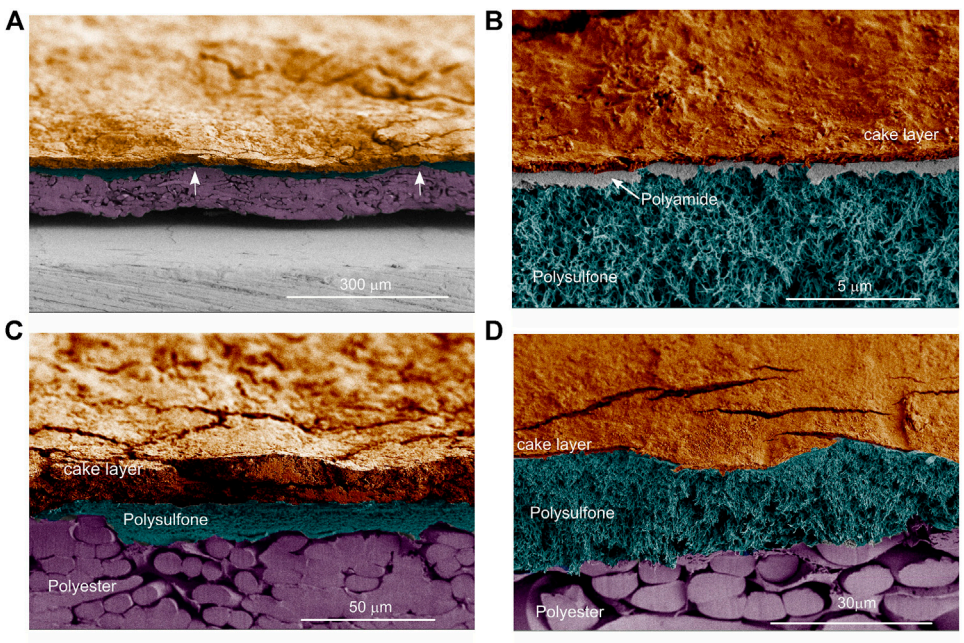

FIGURE 6 | Scanning electron images of cross-sectioned membrane samples. **(A)** A general overview of the membrane and the cake layer. The arrows indicate points where the polysulfone was barely visible along the membrane. **(B)** The polyamide layer is visible, and the cake layer covers the membrane homogenously. **(C)** Compressed polysulfone layer where only the laminar-like polysulfone structure is visible. **(D)** The spongy-like polysulfone structure is visible. Images were pseudo-colored to ease visualizing the distinctive features of the membrane.

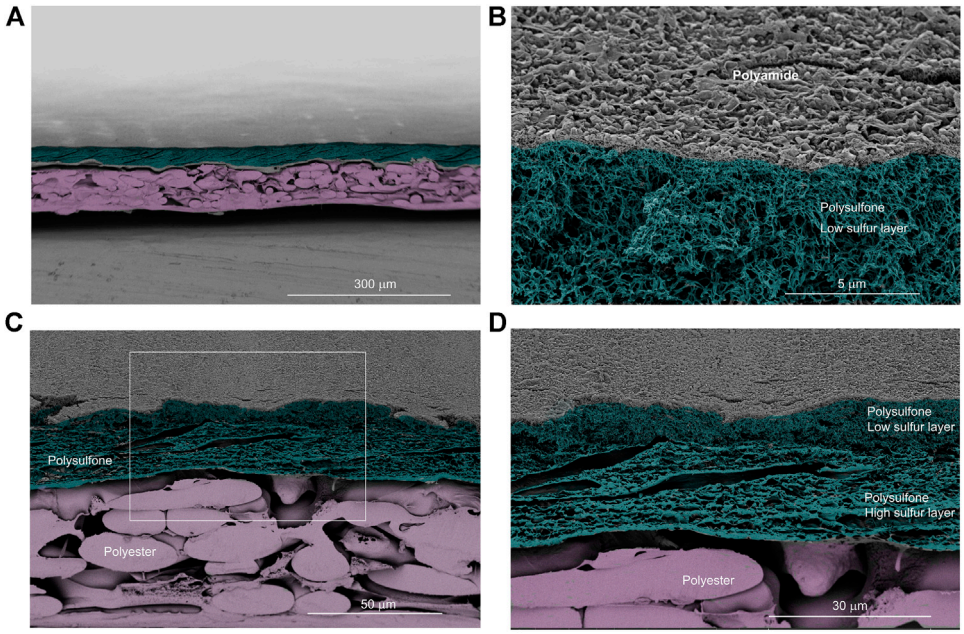

FIGURE 7 | Scanning electron images of cross-sectioned virgin membrane samples. **(A)** A general overview of the membrane. **(B)** The virgin polyamide surface layer is visible, and below this, part of the polysulfone is visible. **(C)** Intact polysulfone layer on top of the polyester layer. **(D)** Zoomed image of the boxed area from panel **(C)** showing the two structures of the polysulfone layer. Images were pseudo-colored to ease visualizing the distinctive features of the membrane.

TABLE 1 | Elemental composition of the fouling material (cake[a]) material of the RO membrane. For comparison, the composition of a clean virgin surface was measured. Moreover, the elemental composition of the two distinct polysulfone layers as shown in **Figure 6D** reveals their contrasting sulfur content. The data was obtained by EDS analysis.

Element	Atomic (%)			
	Fouling cake	Virgin surface	Polysulfone low sulfur layer	Polysulfone high sulfur layer
C	33.6 ± 9.5	70.5 ± 8.3	85.6 ± 0.8	73.3 ± 4.9
N	10.6 ± 1.5	3.6 ± 0.7	0.0 ± 0.0	0.1 ± 0.1
O	32.8 ± 4.5	15.9 ± 3.3	9.7 ± 0.8	5.0 ± 0.8
Mg	1.2 ± 0.3	0.2 ± 0.1	0.1 ± 0.0	0.0 ± 0.0
Al	0.9 ± 0.9	0.3 ± 0.1	1.3 ± 1.0	7.5 ± 1.8
Si	0.5 ± 0.2	0.1 ± 0.1	0.0 ± 0.0	0.0 ± 0.0
S	0.8 ± 0.1	4.5 ± 2.9	2.5 ± 0.5	13.2 ± 3.5
Ca	0.3 ± 0.1	0.0 ± 0.0	0.0 ± 0.0	0.1 ± 0.0
Fe	6.2 ± 1.5	0.1 ± 0.1	0.0 ± 0.0	0.3 ± 0.0

[a]*Inlet cake average values are shown. All elemental composition data can be found in* ***Supplementary Tables S1–S3****.*

TABLE 2 | Ratio of sodium with respect to other main elements found on the membrane.

Elements ratio	Seawater (DOE, 1994)	On membrane estimated by EDS (average, Supplementary Tables S2, S3)	On membrane and spacer estimated by ICP-MS (Supplementary Table S4)
Na/Cl	0.85	1.9 ± 0.2	na[a]
Na/Mg	9	7.6 ± 1.9	7
Na/Ca	45	28.2 ± 5.9	46
Na/K	50	60.0 ± 12	21

[a]*Not analyzed.*

TABLE 3 | Indicators of organic fouling and biofouling from full-scale spiral wound RO installations.

Origin of RO membrane	P drop (mbar)	TOC ($\mu g/cm^2$)	ATP (pg/cm^2)	Cells (counts/cm^2)	Main inorganic foulants: ($\mu g/cm^2$)	Fouling layer thickness (μm)	Main issue and advice given	References
Full scale RO wastewater recycling plant	208[a]	na	6,000	na	na	na	np	Sanawar et al. (2019)
Industrial wastewater recycling plant	na	Na	4,700	na	na	na	np	Filloux et al. (2015)
Full scale RO seawater	na	na	340	na	na	na		Filloux et al. (2015)
Full scale RO groundwater treatment plant	na	na	na	na	$CaCO_3$: nr	na	Antiscalants do not fully avoid precipitation. The membranes are cleaned with citric acid for 9 h	Agnihotri et al. (2020)
Full scale wastewater RO reclamation plants	na	120–280	1,300–11,000	2–12 × 10^{6b}	Ca: 2.5–5.7 Fe: 2.0–6.5		np	Luo et al. (2020)
Full scale RO seawater plant (Australia)	na	20–30	na	na	Na: 10,000 Ca: 2,000–5,000 Fe 1,500–4,000 Si: 1,500	na	np	Jeong et al. (2016)
Full scale NF treating anoxic groundwater	na	4.5–50	150–1,800	na	na	1–2	Natural anoxic conditions of the groundwater prevent Fe deposits and biofouling	Beyer et al. (2014)
15 full scale NF and RO plants (diverse water types)	<10–450	5–150	4–1,02,000	3 × 10^6–1 × 10^9	na	3–91[c]	The normalized pressure drop is not sensitive enough for early detection of fouling	Vrouwenvelder et al. (2008)
46 RO elements from six pilot plants (diverse water types)	na	na	20–45,000	1 × 10^7–2 × 10^9	Fe: 0.1–25 Mn: 0.001–0.2	na	Plants with slow sand filtration as pretreatment have lower risks of fouling	Vrouwenvelder and van der Kooij (2003)
Full scale RO seawater plant (Red Sea)	na	15–23	300–2,800	na	Na: 60–90 Mg: 20–60 Fe: 10–40 Al: 38 Si: 20	na	Filter fibers present on the fouling material. Thus, replace cartridge filter more often	Fortunato et al. (2020)
Full scale RO seawater plant (Red Sea)	2,230	80	10,000	3 × 10^8	Fe: 150	3–20	High Fe content on the fouling layer. Revise Fe chloride coagulat dosage and revise pre-filters replacement schedule	This report, average

na, not analyzed; nr, quantitative value not reported; np, non provided.
[a]*Normalized pressure drop.*
[b]*Measured as heterotrophic plate counts.*
[c]*Data from six plants.*

homogeneous (**Supplementary Tables S3, S4**). The estimated Fe content on the membrane and spacer was 150 $\mu g/cm^2$. This is a high value compared to that reported for a RO membrane treating groundwater, where the Fe was 1–40 $\mu g/cm^2$ using filtered and unfiltered groundwater, respectively (Hijnen et al., 2011). And, Fe contents of about 40 $\mu g/cm^2$ were reported for RO membranes of a desalination plant on the Rea Sea (Fortunato et al., 2020). Iron is a common foulant, and 40% of 99 RO membrane autopsies showed the presence of iron (Chesters et al., 2013). This is because ferric chloride ($FeCl_3$) is one of the most commonly used coagulants in the pretreatment of seawater to remove organic colloids (Al-Sheikh, 1997; Edzwald and Haarhoff, 2011). A recent laboratory study showed that using liquid ferrate, ten times less iron might be required to achieve similar pretreatment efficiencies (Alshahri et al., 2019). However, convincing practitioners to replace $FeCl_3$ with liquid ferrate may need a demonstration of its benefits at pilot scale.

The addition of $FeCl_3$ to waters with natural bicarbonate alkalinity results in the formation of iron hydroxide precipitates. When proper retention of these precipitates prior to the RO system fails, they cause serious inorganic fouling as observed in this membrane. Since the addition of $FeCl_3$ and electrolytes aims at removing suspended solids and colloids, a rational addition of these chemicals should be tightly linked to the online monitoring of turbidity. Residual Fe and electrolytes should be avoided because they could promote fouling—Fe is an essential metal for microbial growth and electrolytes can bind to the RO membrane inducing *in situ* coagulation. Another problem with the presence of iron in the RO membranes is that iron could catalyze the oxidation of the polyamide layer by aqueous chlorine (Gabelich et al., 2002).

Therefore, and based on the diagnosis of this autopsy, we recommend thoroughly 1) revise the extent of iron coagulant dosage, 2) revise the schedule for maintenance of the

pretreatment units (MMF) and replacement of the cartridge filters, and 3) revise the (online) controlling process for coagulant addition. Due to the severity of Fe fouling (**Table 3**), cleaning at this fouling stage might be unpractical, but a cleaning test would be needed for confirmation.

Scanning Electron Microscopy Imaging of Cross-Sectioned Membranes Adds to Autopsies Information

High magnification imaging of cross-sectioned membranes can be a powerful forensic tool. This approach allows accurate measurements of the fouling layer. In addition, the elemental composition of the fouling layer can be readily contrasted to that of the inherent organic structure of the membrane (**Supplementary Tables S3, S4**). This provides added confidence in results particularly when the fouling material is organic. Moreover, cross-sectioned images expose the potential compression of membrane layers. When fouling increases, membranes are operated at increased pressures that result in severe membrane stress. In the studied membrane, we observed zones with high compression of the polysulfone layer (**Figure 6A** *vs.* **Figure 7A**), suggesting that the stress due to operating pressure was heterogeneous. Physical membrane compaction can reflect incomplete cleaning and irreversible fouling (Hoek et al., 2008). Under these conditions, high hydraulic pressures are needed to maintain a desired product water flux (Hoek et al., 2008). The physical compaction in the studied membrane is irreversible as observed by SEM imaging. We did not measure the extent of compaction, but it was reported that compaction could reduce the polysulfone surface porosity by up to ~95% (Davenport et al., 2020). Furthermore, 20–30% of flux is lost due only to polysulfone compaction within 12–20 h after exposure even at low pressures (17 bar) (Hoek et al., 2008). Due to the detrimental effect of membrane compaction on process performance, current studies on spacer configuration aim at minimizing not only biofouling but membrane deformation (Lee et al., 2020).

Improving Autopsies Using New Analytical Methods

New analytical methods to determine the extent of organic fouling and biofouling have advantages over conventional methods. For example, loss-on-ignition is not an accurate measure of the organic matter content in foulant samples with a high proportion of inorganics. This is because of significant reductions of $FeCl_3$ (50%), NH_4Cl, and $(NH_4)_2SO_4$ (both 100%) when the sample is heated at 550°C (da Costa and Schneider, 2019). Simultaneously determining ATP and cell counts seems appropriate for the diagnosis of biofouling (Vrouwenvelder et al., 2008). In particular, the use of flow cytometry to determine cell counts and the extent of biofouling has the advantage of being a high throughput and specific (DNA fluorescence staining) method. This contrast with cell counts via microscopy, which is time-consuming and can be prone to bias. However, biofouling observations via light and fluorescence microscopy provide information about the microbial cell arrangements (i.e., clusters) and coverage. Recently, there is increased interest in assessing the microbial communities of reverse osmosis membranes by high-throughput sequencing (Nagaraj et al., 2017; Rehman et al., 2019). For example, a metagenome study showed that interestingly *Planctomycetes* was the most abundant bacterial phylotype on an RO membrane from a desalination plant on the Red Sea (Rehman et al., 2019). However, how the microbial makeup on full-scale membranes relates to plant operation and how this information can be exploited to better manage (bio)fouling is far from elucidated. For the moment, advanced methods to assess organic fouling and biofouling are mostly used in laboratory investigations using flow cells. However, we anticipate their application as standard methods for autopsies of full-scale RO membrane modules. Here, a word of cautious is pertinent since, in some autopsies, advanced/sophisticated analysis have been used yielding results that are difficult to translate into practice. Unless an autopsy is part of fundamental research efforts, the selection of an array of methods should aim at providing a complete picture of the membrane status to provide rational corrective measures.

The parameters to consider when conducting an autopsy should ideally target all main fouling types. For example, quantification and spatial distribution of inorganic fouling can be assessed by ICP-MS and SEM-EDS, respectively. For the latter, the examination of cross-sectioned samples is recommended since these inform on the thickness of fouling. For organic fouling, measuring TOC seems appropriate, and can be combined with elemental SEM-EDS scans on cross-sectioned samples. From the latter, organic fouling signals are evident since the nitrogen content increases about three times compared to clean membranes (**Table 1**, see also **Supplementary Table S2** *vs.* **Supplementary Tables S3, S4**), and the contents of carbon and oxygen become comparable (i.e., the carbon to oxygen ration approaches one). It should be considered that when fouling appears visually heterogeneous, SEM-EDS observations can be very demanding to acquire a representative overview of fouling. On the other hand, biofouling can be assessed by counting the microbial cells from the membranes using flow cytometry. Although not conducted in this study, this method also allows distinguishing the number of intact (i.e., live) and damaged (i.e., dead) microbial cells. In addition, measuring ATP indicates the presence of active microorganisms. Thus, flow cytometry and ATP estimations are important parameters to include combined when conducting autopsies.

The cake layer of this membrane was relatively compact and thick. However, we consider that it would be advisable to include a brief and gentle rinse of membrane coupons prior to autopsy with filtered sterile ultrapure water to remove any remnant process water, which could influence results particularly in the case of low fouled membranes. The brief and gentle rinse might be dipping the coupon a couple of seconds in the ultrapure water.

Do We Need More Autopsies?

The need for autopsies would be limited when fouling was better understood allowing improved management of fouling issues in full-scale plants. Since fouling is still an important issue in full-

scale installations, membrane autopsies are still required. Currently, most autopsies published refer to laboratory-scale studies with biodegradable nutrient dosage to accelerate fouling. One main limitation of laboratory-scale studies is the difficulty translating the gained information to real systems. For example, chemical cleaning efficiencies in full-scale reverse osmosis membranes are lower than when investigated under laboratory conditions (Jafari et al., 2020). This highlights the need for full-scale research and reporting of data. Unfortunately, autopsies from full-scale membranes are limited. Certainly, practitioners conduct membrane autopsies. However, the information is not in the public literature. Ideally, besides being published, results of full-scale membrane autopsies along with information of key process parameters, water quality and dosed chemicals, could be archived in a public database. One can envision such a database to serve as a diagnostic and corrective tool in a similar manner as medical databases are used by medical practitioners to diagnose and medicate patients. This idea highlights the need for a consensus procedure for conducting autopsies and reporting data. Finally, we propose that a scale to determine the degree of fouling could be constructed based on the above-mentioned database. In such a scale, degrees of fouling from mild to severe could be associated to defined indicators.

CONCLUSION

There is a need for reporting of autopsy research. To maximize data mining, the reports should include process and performance data, a diagnosis, and prevention and control propositions. Furthermore, a consensus procedure for full-scale membrane autopsies would be helpful to allow comparisons between studies.

We demonstrated that with the procedure used in this case study it was possible to investigate different types of fouling simultaneously. A diagnosis was possible and recommendations to address the problem were provided.

The autopsy showed that the membrane module from a full-scale seawater desalination plant characterized by reduced performance indicators (a feed channel pressure drop increase of about 218%) showcased biofouling (up to 21,000 pg ATP/cm2, up to 7×10^8 cells/cm^2), organic fouling (up to 98 μg TOC/cm^2) and iron accumulation (150 μg/cm^2) as well as irreversible membrane compaction.

Based on our findings, we advise a thorough revision of iron coagulant dosage and a revised schedule for the maintenance and replacement of the pre-filter units. Cleaning of membranes having the level of fouling as found in this membrane seems unpractical, but a cleaning test would be required to assess its feasibility.

Finally, it would be valuable to build a RO membrane database, which can be used as a guidance and diagnostic tool for experts and practitioners in this field.

DATA AVAILABILITY STATEMENT

The original contributions presented in the study are included in the article/**Supplementary Material**, further inquiries can be directed to the corresponding author.

AUTHOR CONTRIBUTIONS

GG-G and JV contributed to conception and design of the study. PB retrieved the full-scale module. PB, SB and GG-G conducted the module opening and sampling. AB and GG-G designed SEM work approach. AB conducted SEM-EDS analyses. GG-G conducted TOC, FCM and ATP analyses. AF conducted FT-IR analyses. CZ conducted ICP-MS analyses. TN, RD and TA contributed with plant operation data. GG-G organized and analyzed data set and wrote the draft manuscript. All authors contributed to discussions and manuscript revision, read, and approved the submitted version.

FUNDING

This research was supported by King Abdullah University of Science and Technology (KAUST), Saudi Arabia.

ACKNOWLEDGMENTS

We thank Vitor Borges for his help during the transport and the opening of the membrane module.

SUPPLEMENTARY MATERIAL

The Supplementary Material for this article can be found online at: https://www.frontiersin.org/articles/10.3389/fceng.2021.683379/full#supplementary-material

REFERENCES

DOE (1994). *Handbook of Methods for the Analysis of the Various Parameters of the Carbon Dioxide System in Sea Water*. Editors A. G. Dickson, and C. Goyet. version 2 (Oak Ridge, TN: ORNL/CDIAC-74).

Agnihotri, B., Sharma, A., and Gupta, A. B. (2020). Characterization and Analysis of Inorganic Foulants in RO Membranes for Groundwater Treatment. *Desalination* 491, 114567. doi:10.1016/j.desal.2020.114567

Al-Sheikh, A. H. H. (1997). Seawater Reverse Osmosis Pretreatment with an Emphasis on the Jeddah Plant Operation Experience. *Desalination* 110 (1), 183–192. doi:10.1016/s0011-9164(97)00096-9

Alshahri, A. H., Fortunato, L., Ghaffour, N., and Leiknes, T. (2019). Advanced Coagulation Using *In-Situ* Generated Liquid Ferrate, Fe (VI), for Enhanced Pretreatment in Seawater RO Desalination during Algal Blooms. *Sci. Total Environ.* 685, 1193–1200. doi:10.1016/j.scitotenv.2019.06.286

Alvarez, J., Saudino, G., Musteata, V., Madhavan, P., Genovese, A., Behzad, A. R., et al. (2019). 3D Analysis of Ordered Porous Polymeric Particles Using Complementary Electron Microscopy Methods. *Scientific Rep.* 9 (1), 13987. doi:10.1038/s41598-019-50338-2

Beyer, F., Rietman, B. M., Zwijnenburg, A., van den Brink, P., Vrouwenvelder, J. S., Jarzembowska, M., et al. (2014). Long-term Performance and Fouling Analysis of Full-Scale Direct Nanofiltration (NF) Installations Treating Anoxic Groundwater. *J. Membr. Sci.* 468, 339–348. doi:10.1016/j.memsci.2014.06.004

Bristow, N. W., Vogt, S. J., Bucs, S. S., Vrouwenvelder, J. S., Johns, M. L., and Fridjonsson, E. O. (2021). Novel Magnetic Resonance Measurements of Fouling in Operating Spiral Wound Reverse Osmosis Membrane Modules. *Water Res.* 196, 117006. doi:10.1016/j.watres.2021.117006

Carnahan, R. P., Bolin, L., and Suratt, W. (1995). Biofouling of PVD-1 Reverse Osmosis Elements in the Water Treatment Plant of the City of Dunedin, Florida. *Desalination* 102 (1), 235–244. doi:10.1016/0011-9164(95)00059-b

Chesters, S. P., Pena, N., Gallego, S., Fazel, M., Armstrong, M. W., and del Vigo, F. (2013). Results from 99 Seawater RO Membrane Autopsies. *IDA. J. Desalination Water Reuse* 5 (1), 40–47. doi:10.1179/2051645213y.0000000006

Chong, T., Wong, F., and Fane, A. (2008). The Effect of Imposed Flux on Biofouling in Reverse Osmosis: Role of Concentration Polarisation and Biofilm Enhanced Osmotic Pressure Phenomena. *J. Membr. Sci.* 325 (2), 840–850. doi:10.1016/j.memsci.2008.09.011

Creber, S. A., Pintelon, T. R. R., Graf von der Schulenburg, D. A. W., Vrouwenvelder, J. S., van Loosdrecht, M. C. M., and Johns, M. L. (2010a). Magnetic Resonance Imaging and 3D Simulation Studies of Biofilm Accumulation and Cleaning on Reverse Osmosis Membranes. *Food Bioproducts Process.* 88 (4), 401–408. doi:10.1016/j.fbp.2010.08.010

Creber, S. A., Vrouwenvelder, J. S., van Loosdrecht, M. C. M., and Johns, M. L. (2010b). Chemical Cleaning of Biofouling in Reverse Osmosis Membranes Evaluated Using Magnetic Resonance Imaging. *J. Membr. Sci.* 362 (1), 202–210. doi:10.1016/j.memsci.2010.06.052

da Costa, T. R., and Schneider, R. P. (2019). Critical Evaluation of Procedures Fundamental to Reverse Osmosis Membrane Autopsy. *Dwt* 154, 49–62. doi:10.5004/dwt.2019.24112

Darton, T., Annunziata, U., del Vigo Pisano, F., and Gallego, S. (2004). Membrane Autopsy Helps to Provide Solutions to Operational Problems. *Desalination* 167, 239–245. doi:10.1016/j.desal.2004.06.133

Davenport, D. M., Ritt, C. L., Verbeke, R., Dickmann, M., Egger, W., Vankelecom, I. F. J., et al. (2020). Thin Film Composite Membrane Compaction in High-Pressure Reverse Osmosis. *J. Membr. Sci.* 610, 118268. doi:10.1016/j.memsci.2020.118268

Dudley, L. Y., and Darton, E. G. (1996). Membrane Autopsy - a Case Study. *Desalination* 105 (1), 135–141. doi:10.1016/0011-9164(96)00067-7

Eberle, A. L., and Zeidler, D. (2018). Multi-Beam Scanning Electron Microscopy for High-Throughput Imaging in Connectomics Research. *Front. Neuroanat.* 12 (112). doi:10.3389/fnana.2018.00112

Edzwald, J. K., and Haarhoff, J. (2011). Seawater Pretreatment for Reverse Osmosis: Chemistry, Contaminants, and Coagulation. *Water Res.* 45 (17), 5428–5440. doi:10.1016/j.watres.2011.08.014

Filloux, E., Wang, J., Pidou, M., Gernjak, W., and Yuan, Z. (2015). Biofouling and Scaling Control of Reverse Osmosis Membrane Using One-step Cleaning-Potential of Acidified Nitrite Solution as an Agent. *J. Membr. Sci.* 495, 276–283. doi:10.1016/j.memsci.2015.08.034

Flemming, H.-C. (2020). Biofouling and Me: My Stockholm Syndrome with Biofilms. *Water Res.* 173, 115576. doi:10.1016/j.watres.2020.115576

Fortunato, L., Alshahri, A. H., Farinha, A. S. F., Zakzouk, I., Jeong, S., and Leiknes, T. (2020). Fouling Investigation of a Full-Scale Seawater Reverse Osmosis Desalination (SWRO) Plant on the Red Sea: Membrane Autopsy and Pretreatment Efficiency. *Desalination* 496, 114536. doi:10.1016/j.desal.2020.114536

Gabelich, C. J., Yun, T. I., Coffey, B. M., and Suffet, I. H. M. (2002). Effects of Aluminum Sulfate and Ferric Chloride Coagulant Residuals on Polyamide Membrane Performance. *Desalination* 150 (1), 15–30. doi:10.1016/s0011-9164(02)00926-8

Griebe, T., and Flemming, H.-C. (1998). Biocide-free Antifouling Strategy to Protect RO Membranes from Biofouling. *Desalination* 118 (1), 153–IN9. doi:10.1016/s0011-9164(98)00113-1

Hammes, F., Goldschmidt, F., Vital, M., Wang, Y., and Egli, T. (2010). Measurement and Interpretation of Microbial Adenosine Tri-phosphate (ATP) in Aquatic Environments. *Water Res.* 44 (13), 3915–3923. doi:10.1016/j.watres.2010.04.015

Herzberg, M., and Elimelech, M. (2007). Biofouling of Reverse Osmosis Membranes: Role of Biofilm-Enhanced Osmotic Pressure. *J. Membr. Sci.* 295 (1), 11–20. doi:10.1016/j.memsci.2007.02.024

Hijnen, W. A. M., Biraud, D., Cornelissen, E. R., and van der Kooij, D. (2009). Threshold Concentration of Easily Assimilable Organic Carbon in Feedwater for Biofouling of Spiral-Wound Membranes. *Environ. Sci. Technol.* 43 (13), 4890–4895. doi:10.1021/es900037x

Hijnen, W. A. M., Cornelissen, E. R., and van der Kooij, D. (2011). Threshold Concentrations of Biomass and Iron for Pressure Drop Increase in Spiral-Wound Membrane Elements. *Water Res.* 45 (4), 1607–1616. doi:10.1016/j.watres.2010.11.047

Hoek, E. M. V., Allred, J., Knoell, T., and Jeong, B.-H. (2008). Modeling the Effects of Fouling on Full-Scale Reverse Osmosis Processes. *J. Membr. Sci.* 314 (1), 33–49. doi:10.1016/j.memsci.2008.01.025

Hugenholtz, P. (2002). Exploring Prokaryotic Diversity in the Genomic Era. *Genome Biol.* 3 (2), reviews0003. doi:10.1186/gb-2002-3-2-reviews0003

Jafari, M., D'Haese, A., Zlopasa, J., Cornelissen, E. R., Vrouwenvelder, J. S., Verbeken, K., et al. (2020). A Comparison between Chemical Cleaning Efficiency in Lab-Scale and Full-Scale Reverse Osmosis Membranes: Role of Extracellular Polymeric Substances (EPS). *J. Membr. Sci.* 609, 118189. doi:10.1016/j.memsci.2020.118189

Jeong, S., Naidu, G., Vollprecht, R., Leiknes, T., and Vigneswaran, S. (2016). In-depth Analyses of Organic Matters in a Full-Scale Seawater Desalination Plant and an Autopsy of Reverse Osmosis Membrane. *Sep. Purif. Tech.* 162, 171–179. doi:10.1016/j.seppur.2016.02.029

Jiang, S., Li, Y., and Ladewig, B. P. (2017). A Review of Reverse Osmosis Membrane Fouling and Control Strategies. *Sci. Total Environ.* 595, 567–583. doi:10.1016/j.scitotenv.2017.03.235

Jones, E., Qadir, M., van Vliet, M. T. H., Smakhtin, V., and Kang, S.-m. (2019). The State of Desalination and Brine Production: A Global Outlook. *Sci. Total Environ.* 657, 1343–1356. doi:10.1016/j.scitotenv.2018.12.076

Kerdi, S., Qamar, A., Alpatova, A., Vrouwenvelder, J. S., and Ghaffour, N. (2020). Membrane Filtration Performance Enhancement and Biofouling Mitigation Using Symmetric Spacers with Helical Filaments. *Desalination* 484, 114454. doi:10.1016/j.desal.2020.114454

Kucera, J. (2019). Biofouling of Polyamide Membranes: Fouling Mechanisms, Current Mitigation and Cleaning Strategies, and Future Prospects. *Membranes* 9 (9), 111. doi:10.3390/membranes9090111

Lee, C., Jang, J., Tin, N. T., Kim, S., Tang, C. Y., and Kim, I. S. (2020). Effect of Spacer Configuration on the Characteristics of FO Membranes: Alteration of Permeation Characteristics by Membrane Deformation and Concentration Polarization. *Environ. Sci. Technol.* 54 (10), 6385–6395. doi:10.1021/acs.est.9b06921

Liu, G., Pattanayak, S., Navaneethakrishnan, P., and Woodling, R. (2018). Role of Membrane Autopsy in Enhancing Reverse Osmosis Plant Operation. *Water Pract. Tech.* 13 (1), 106–114. doi:10.2166/wpt.2018.020

Luo, H., Cui, Y., Zhang, H., Li, C., Wang, Z., and Song, P. (2020). Analyzing and Verifying the Association of Spiral-Wound Reverse Osmosis Membrane Fouling with Different Secondary Effluents: Full-Scale Experiments. *Sci. Total Environ.* 711, 135150. doi:10.1016/j.scitotenv.2019.135150

Mazlan, N. M., Peshev, D., and Livingston, A. G. (2016). Energy Consumption for Desalination - A Comparison of Forward Osmosis with Reverse Osmosis, and the Potential for Perfect Membranes. *Desalination* 377, 138–151. doi:10.1016/j.desal.2015.08.011

Nagaraj, V., Skillman, L., Ho, G., Li, D., and Gofton, A. (2017). Characterisation and Comparison of Bacterial Communities on Reverse Osmosis Membranes of a Full-Scale Desalination Plant by Bacterial 16S rRNA Gene Metabarcoding. *npj Biofilms and Microbiomes* 3 (1), 13. doi:10.1038/s41522-017-0021-6

Nejati, S., Mirbagheri, S. A., Warsinger, D. M., and Fazeli, M. (2019). Biofouling in Seawater Reverse Osmosis (SWRO): Impact of Module Geometry and Mitigation with Ultrafiltration. *J. Water Process Eng.* 29, 100782. doi:10.1016/j.jwpe.2019.100782

Nescerecka, A., Hammes, F., and Juhna, T. (2016). A Pipeline for Developing and Testing Staining Protocols for Flow Cytometry, Demonstrated with SYBR Green I and Propidium Iodide Viability Staining. *J. Microbiol. Methods* 131, 172–180. doi:10.1016/j.mimet.2016.10.022

Peña, N., Gallego, S., del Vigo, F., and Chesters, S. P. (2013). Evaluating Impact of Fouling on Reverse Osmosis Membranes Performance. *Desalination Water Treat.* 51 (4-6), 958–968. doi:10.1080/19443994.2012.699509

Petersen, R. J. (1993). Composite Reverse Osmosis and Nanofiltration Membranes. *J. Membr. Sci.* 83 (1), 81–150. doi:10.1016/0376-7388(93)80014-o

Prest, E. I., Hammes, F., Kötzsch, S., van Loosdrecht, M. C. M., and Vrouwenvelder, J. S. (2013). Monitoring Microbiological Changes in Drinking Water Systems

Using a Fast and Reproducible Flow Cytometric Method. *Water Res.* 47 (19), 7131–7142. doi:10.1016/j.watres.2013.07.051

Qamar, A., Kerdi, S., Ali, S. M., Shon, H. K., Vrouwenvelder, J. S., and Ghaffour, N. (2021). Novel Hole-Pillar Spacer Design for Improved Hydrodynamics and Biofouling Mitigation in Membrane Filtration. *Scientific Rep.* 11 (1), 6979. doi:10.1038/s41598-021-86459-w

Qasim, M., Badrelzaman, M., Darwish, N. N., Darwish, N. A., and Hilal, N. (2019). Reverse Osmosis Desalination: A State-Of-The-Art Review. *Desalination* 459, 59–104. doi:10.1016/j.desal.2019.02.008

Radu, A. I., Vrouwenvelder, J. S., van Loosdrecht, M. C. M., and Picioreanu, C. (2010). Modeling the Effect of Biofilm Formation on Reverse Osmosis Performance: Flux, Feed Channel Pressure Drop and Solute Passage. *J. Membr. Sci.* 365 (1), 1–15. doi:10.1016/j.memsci.2010.07.036

Rehman, Z. U., Ali, M., Iftikhar, H., and Leiknes, T. (2019). Genome-resolved Metagenomic Analysis Reveals Roles of Microbial Community Members in Full-Scale Seawater Reverse Osmosis Plant. *Water Res.* 149, 263–271. doi:10.1016/j.watres.2018.11.012

Rho, H., Chon, K., and Cho, J. (2019). An Autopsy Study of a Fouled Reverse Osmosis Membrane Used for Ultrapure Water Production. *Water* 11 (6), 1116. doi:10.3390/w11061116

Rodríguez-Calvo, A., Silva-Castro, G. A., Osorio, F., González-López, J., and Calvo, C. (2015). Reverse Osmosis Seawater Desalination: Current Status of Membrane Systems. *Desalination Water Treat.* 56 (4), 849–861. doi:10.1080/19443994.2014.942378

Ruiz-García, A., Melián-Martel, N., and Mena, V. (2018). Fouling Characterization of RO Membranes after 11 Years of Operation in a Brackish Water Desalination Plant. *Desalination* 430, 180–185. doi:10.1016/j.desal.2017.12.046

Ruiz-García, A., and Ruiz-Saavedra, E. (2015). 80,000h Operational Experience and Performance Analysis of a Brackish Water Reverse Osmosis Desalination Plant. Assessment of Membrane Replacement Cost. *Desalination* 375, 81–88. doi:10.1016/j.desal.2015.07.022

Sanawar, H., Bucs, S. S., Pot, M. A., Zlopasa, J., Farhat, N. M., Witkamp, G.-J., et al. (2019). Pilot-Scale Assessment of Urea as a Chemical Cleaning Agent for Biofouling Control in Spiral-Wound Reverse Osmosis Membrane Elements. *Membranes (Basel)* 9, 117. doi:10.3390/membranes9090117

Siddiqui, A., Lehmann, S., Bucs, S. S., Fresquet, M., Fel, L., Prest, E. I. E. C., et al. (2017). Predicting the Impact of Feed Spacer Modification on Biofouling by Hydraulic Characterization and Biofouling Studies in Membrane Fouling Simulators. *Water Res.* 110, 281–287. doi:10.1016/j.watres.2016.12.034

Siebdrath, N., Farhat, N., Ding, W., Kruithof, J., and Vrouwenvelder, J. S. (2019). Impact of Membrane Biofouling in the Sequential Development of Performance Indicators: Feed Channel Pressure Drop, Permeability, and Salt Rejection. *J. Membr. Sci.* 585, 199–207. doi:10.1016/j.memsci.2019.05.043

Sundaramoorthi, G., Hadwiger, M., Ben-Romdhane, M., Behzad, A. R., Madhavan, P., and Nunes, S. P. (2016). 3D Membrane Imaging and Porosity Visualization. *Ind. Eng. Chem. Res.* 55 (12), 3689–3695. doi:10.1021/acs.iecr.6b00387

Tawalbeh, M., Al Mojjly, A., Al-Othman, A., and Hilal, N. (2018). Membrane Separation as a Pre-treatment Process for Oily saline Water. *Desalination* 447, 182–202. doi:10.1016/j.desal.2018.07.029

UNESCO UN-Water (2020). *United Nations World Water Development Report 2020: Water and Climate Change*. Paris: UNESCO.

Van Nevel, S., Koetzsch, S., Proctor, C. R., Besmer, M. D., Prest, E. I., Vrouwenvelder, J. S., et al. (2017). Flow Cytometric Bacterial Cell Counts challenge Conventional Heterotrophic Plate Counts for Routine Microbiological Drinking Water Monitoring. *Water Res.* 113, 191–206. doi:10.1016/j.watres.2017.01.065

Voutchkov, N. (2010). Introduction to Reverse Osmosis Desalination. *A SunCam Online Continuing Education Course*. Florida: SunCam, Inc. Available at www.suncam.com/authors/110Voutchkov/053.pdf.

Vrede, K., Heldal, M., Norland, S., and Bratbak, G. (2002). Elemental Composition (C, N, P) and Cell Volume of Exponentially Growing and Nutrient-Limited Bacterioplankton. *Aem* 68 (6), 2965–2971. doi:10.1128/aem.68.6.2965-2971.2002

Vrouwenvelder, J. S., Hinrichs, C., Van der Meer, W. G. J., Van Loosdrecht, M. C. M., and Kruithof, J. C. (2009). Pressure Drop Increase by Biofilm Accumulation in Spiral Wound RO and NF Membrane Systems: Role of Substrate Concentration, Flow Velocity, Substrate Load and Flow Direction. *Biofouling* 25 (6), 543–555. doi:10.1080/08927010902972225

Vrouwenvelder, J. S., Kappelhof, J. W. N. M., Heijrnan, S. G. J., Schippers, J. C., and van der Kooija, D. (2003). Tools for Fouling Diagnosis of NF and RO Membranes and Assessment of the Fouling Potential of Feed Water. *Desalination* 157 (1), 361–365. doi:10.1016/s0011-9164(03)00417-x

Vrouwenvelder, J. S., Manolarakis, S. A., van der Hoek, J. P., van Paassen, J. A. M., van der Meer, W. G. J., van Agtmaal, J. M. C., et al. (2008). Quantitative Biofouling Diagnosis in Full Scale Nanofiltration and Reverse Osmosis Installations. *Water Res.* 42 (19), 4856–4868. doi:10.1016/j.watres.2008.09.002

Vrouwenvelder, J. S., Manolarakis, S. A., Veenendaal, H. R., and van der Kooij, D. (2000). Biofouling Potential of Chemicals Used for Scale Control in RO and NF Membranes. *Desalination* 132 (1), 1–10. doi:10.1016/s0011-9164(00)00129-6

Vrouwenvelder, J. S., and van der Kooij, D. (2003). Diagnosis of Fouling Problems of NF and RO Membrane Installations by a Quick Scan. *Desalination* 153 (1), 121–124. doi:10.1016/s0011-9164(02)01111-6

Vrouwenvelder, J. S., van Loosdrecht, M. C. M., and Kruithof, J. C. (2011). Early Warning of Biofouling in Spiral Wound Nanofiltration and Reverse Osmosis Membranes. *Desalination* 265 (1), 206–212. doi:10.1016/j.desal.2010.07.053

Zargar, M., Ujihara, R., Vogt, S. J., Vrouwenvelder, J. S., Fridjonsson, E. O., and Johns, M. L. (2020). Imaging of Membrane Concentration Polarization by NaCl Using 23Na Nuclear Magnetic Resonance. *J. Membr. Sci.* 600, 117868. doi:10.1016/j.memsci.2020.117868

Zheng, L., Yu, D., Wang, G., Yue, Z., Zhang, C., Wang, Y., et al. (2018). Characteristics and Formation Mechanism of Membrane Fouling in a Full-Scale RO Wastewater Reclamation Process: Membrane Autopsy and Fouling Characterization. *J. Membr. Sci.* 563, 843–856. doi:10.1016/j.memsci.2018.06.043

Conflict of Interest: Authors AZ and RD were employed by the company NOMAC. Author TA was employed by the company ACWA Power Innovation Department.

The remaining authors declare that the research was conducted in the absence of any commercial or financial relationships that could be construed as a potential conflict of interest.